Journal of Environmental Protection, 2023, 14, 16-31
https://www.scirp.org/journal/jep
ISSN Online: 2152-2219
ISSN Print: 2152-2197

Optimization of Preparation Conditions of Modified Oyster Shell Powder/Ce-N-TiO_2 by Response Surface Methodology (RSM)

Wei Zhang[1,2,3], Qizheng You[2*], Jinkai Shu[1,3], Aihe Wang[1,3], Hai Lin[4], Xuchao Yan[4]

[1]School of Municipal and Mapping Engineer, Hunan City University, Yiyang, China
[2]School of Municipal and Environmental Engineering, Shenyang Jianzhu University, Shenyang, China
[3]Hunan Provincial Village Drinking Water Quality Safety Engineering Technology Research Center, Yiyang, China
[4]Yiyang City Commodity Quality Supervision and Inspection Institute, Yiyang, China
Email: *1140235363@qq.com

How to cite this paper: Zhang, W., You, Q.Z., Shu, J.K., Wang, A.H., Lin, H. and Yan, X.C. (2023) Optimization of Preparation Conditions of Modified Oyster Shell Powder/Ce-N-TiO_2 by Response Surface Methodology (RSM). *Journal of Environmental Protection*, **14**, 16-31.
https://doi.org/10.4236/jep.2023.141002

Received: December 5, 2022
Accepted: January 8, 2023
Published: January 11, 2023

Abstract

A new composite photocatalyst of modified oyster shell powder/Ce-N-TiO_2 was prepared by sol-gel method. Based on single factor experiment, Ce doping rate, N doping rate and calcination temperature were taken as input variables. Based on the central composite design (BBD) response surface model, two functional relationship models between three independent variables and glyphosate removal rate were established to evaluate the influence degree of independent variables and interaction on catalyst. The significance of the model and regression coefficient was tested by variance analysis. The analysis of the obtained data showed that the degradation performance of the composite photocatalyst was significantly affected by the calcination temperature and the rate of N doping, while the rate of Ce doping had little effect; at the calcination temperature of 505.440˚C, the degradation rate of glyphosate reached the maximum of 82.15% under the preparation conditions of 17.057 mol% N doping and 0.165 mol% Ce doping, respectively.

Keywords

Modified Titanium Dioxide, Response Surface Methodology (RSM), Photocatalysis, Glyphosate

1. Introduction

Glyphosate (N-(Phosphonomethyl) glycine, PMG) is one of the most widely used broad-spectrum active organophosphorus herbicides in the world [1], reaching a solubility of 15.7 g/L (pH = 7) in water at 25˚C. In recent years, with the devel-

opment of agriculture and industry, the intensive use of glyphosate pesticides on a large scale has made it an important component of DOP input to the water environment through the surface water circulation system, with significant toxic effects on phytoplankton, fish and other aquatic organisms in the water column [2]. In view of the harmful side effects of glyphosate and its derivative AMPA on soil and water quality as well as plant, animal and human health, it has been reclassified as a possible carcinogen by the World Health Organization in 2015 based on reports of potential chronic side effects of glyphosate in recent years [3] [4] [5].

In recent years, photocatalytic technology has shown great promise for the degradation of various persistent and toxic organic pollutants in water bodies [6] [7] [8]. Among them, TiO_2 is the most widely used photocatalyst, however, its low light absorption capacity and high electron-hole pair loading rate directly limit its photocatalytic activity and further engineering applications [9]. In recent years, researchers have used various approaches to improve their photocatalytic activity, such as surface modification of noble metals, doping with metal or non-metal ions, and synthesis of different nanostructures, among which, co-doping with different metal or non-metal ions is considered as one of the most effective strategies to improve photocatalytic performance. For example, modified TiO_2 photocatalysts such as Ce-TiO_2 [10], C-N-S-TiO_2 [11] and Fe-N-TiO_2 [12] have been explored and studied for their mechanism of pollutant degradation. However, the low adsorption capacity of the suspension-modified TiO_2 alone resulted in its photocatalytic degradation of pollutants and could not be further enhanced.

Further, combining TiO_2 photocatalysts with efficient adsorbent materials may enhance their ability to degrade pollutants, which is mainly attributed to the synergistic effect of adsorption and photocatalysis [13]. The adsorbent may adsorb a large number of organic pollutant molecules, thus facilitating the reaction between the organic molecules and the active radicals formed on the TiO_2 surface, forming an adsorption-catalysis photodegradation pathway. Currently, the use of waste materials to prepare new, inexpensive, "green" adsorbents is a hot research topic [14] [15], such as quartz particles, fly ash, zeolite, and other natural materials and waste residue-based adsorbent materials [16] [17] [18] [19]. However, there are not many reports on the preparation of composite photocatalysts with adsorption-photocatalytic synergy by combining the above-mentioned types of adsorbent materials with modified TiO_2.

In this study, cerium metal and non-metallic nitrogen were doped into titanium dioxide by sol-gel method, based on this research team's study of modified oyster shell powder prepared by processing and modification of natural oyster shell as raw material, the Ce-N-TiO_2 photocatalyst was loaded onto the modified oyster shell powder to form a modified oyster shell powder/Ce-N-TiO_2 composite photocatalyst. The effect of the preparation conditions on the degradation of glyphosate was analyzed on the basis of a single-factor test, and the suitability of the composite photocatalyst for the removal of glyphosate was assessed by para-

meter optimization and modelling using the response surface methodology (RSM). The model was validated for reasonableness.

2. Materials and Methods

2.1. Materials

Discarded oyster shells, Glyphosate (N-(Phosphonomethyl) glycine, $C_3H_8NO_5P$, 95%) was from Shi-Feng Biotechnology Co. Ltd, Shanghai, PRC; Tetrabutyl orthotitanate (TBOT), Absolute ethanol (C_2H_5OH) as solvent, Cerium nitrate hexahydrate ($Ce(NO_3)_3{\cdot}6H_2O$) and urea (CH_4N_2O) were used as the source of cerium and nitrogen, respectively, hydrochloric acid (HCl). All chemicals were analytical grade purity and can be directly applied without any further treatment.

2.2. Photocatalyst Preparation

2.2.1. Preparation of Modified Oyster Shell Powder

The surface residue of waste oyster shells was cleaned with detergent and cleaning ball, and the surface was polished to white with cutting machine and cut into small pieces, dried at 65˚C in blast drying oven and crushed in sealed sample making machine, sieved at 120 mesh, then soaked in 0.1% HCl, vacuum dried and calcined at 900˚C for 2 h in muffle furnace to obtain modified oyster shell powder, sealed and kept for backup.

2.2.2. Preparation of Modified Oyster Shell Powder/Ce-N-TiO_2

Measure 36 mL of anhydrous ethanol and quantitative modified oyster shell powder mixed with ultrasonic shaking for 10 mins, then under the action of magnetic stirring, tetrabutyl titanate was added to the above mixture drop by drop at a rate of 1 - 2 drops/s and stirred evenly for 20 min to form solution A; Measure 36 mL of anhydrous ethanol, 3.0 mL of distilled water, 0.2 mL of hydrochloric acid and mix thoroughly, add a certain rate of urea and cerium nitrate hexahydrate, and form solution B by ultrasonic shaking for 10 min. The solution B was slowly added dropwise to the above solution A at a rate of 30 - 35 drops/min and stirred until a uniform transparent sol was formed. After aging in a vacuum drying oven at 25˚C for 24 hours, it was put into a blast dryer at 85˚C for overnight drying, crushed, and finally calcined in a muffle furnace at a certain temperature for 2 h to form the modified oyster shell powder/Ce-N-TiO_2 composite photocatalyst. Alternatively, the method of preparing the Ce-N-TiO_2 photocatalyst is the same as that described above except that the modified oyster shell powder is not added.

2.3. Photocatalytic Activity Measurement

To investigate the photocatalytic activity of modified oyster shell powder/Ce-N-TiO_2, photodegradation tests were carried out on glyphosate solutions under simulated daylight xenon lamps. 100 mg of catalyst was dispersed into 100 mL of glyphosate solution, where the initial glyphosate concentration was 50 mg/L and the pH was adjusted to between 2 and 3. The mixture was magnetically stirred in

a dark room to achieve complete adsorption-desorption equilibrium before the light source was switched on. The xenon lamp light source was then switched on and the appropriate power adjusted. 3 mL of the sample was taken after each time interval and the supernatant was centrifuged to determine the PO_4^{3-} concentration and calculate the organophosphorus degradation rate of the glyphosate solution. The formula is shown in Equation (1).

$$\eta(\%) = \frac{C_t}{C_o} \times 100\% \quad (1)$$

η—organophosphorus degradation rate in glyphosate;
C_t— PO_4^{3-} content in glyphosate at moment t, mg/L;
C_o—Total phosphorus content in glyphosate at the initial moment, mg/L.

2.4. Experimental Design

Based on the previous research of the subject group, three main influencing factors, namely Ce doping rate, N doping rate and calcination temperature, were selected to investigate the effect of modified oyster shell powder/Ce-N-TiO_2 composite photocatalyst in the degradation of PMG solution by simulated sunlight and to analyze the reasons for it. In order to determine the optimal preparation conditions for the degradation of PMG solution by modified oyster shell powder/Ce-N-TiO_2, as well as to analyse the degree of influence of each factor on the experimental results, the optimized variable values were determined through the above experiments, based on Design Eepert 11.0 software, combined with the central combination design (BBD) response surface test scheme, as shown in Table 1.

3. Results and Discussion

3.1. Single-Factor Experiment

3.1.1. Effect of Ce Doping Rate on Photocatalytic Degradation

It can be seen from Figure 1 that the degradation rate of PMG increases with the increase of Ce doping rate. When the Ce doping rate is 0.1 mol%, the maximum degradation rate is 79.5%, and when the Ce doping rate increases to 1.0 mol%, the degradation rate of glyphosate decreases to 52%. The results show that, there is an optimal doping value for cerium doped with different photocatalysts. Ce

Table 1. Process variables and their experimental levels.

Factor name	Code	Units	Range and levels			
			Actual		Coded	
			Low	High	Low	High
N doping	X_1	mol%	10	50	−1.000	1.000
Ce dopiong	X_2	mol%	0.1	0.3	−1.000	1.000
Calcination temperature	X_3	˚C	450	550	−1.000	1.000

doping makes Ce^{3+} and Ce^{4+} coexist on the crystal surface or gap. Ce^{3+}/Ce^{4+} is called "oxygen tank" because of its special redox performance [20]. Ce^{4+} has strong electron capture ability to improve the separation efficiency of photogenerated e^-/h^+ pairs, while Ce^{3+} can absorb oxygen to form superoxide radicals to participate in the photocatalytic reaction, as shown in Equation (2) and Equation (3). However, with the increase of cerium doping rate, the TiO_2 anatase lattice will cause structural changes, which will instead produce the compound phenomenon of photogenerated e^-/h^+ pairs [21], thus reducing its photodegradation activity to PMG.

$$Ce^{4+} + e^- \rightarrow Ce^{3+} \tag{2}$$

$$Ce^{3+} + O_2 \rightarrow {}^{\bullet}O_2^- + Ce^{4+} \tag{3}$$

3.1.2. Effect of N Doping Rate on Photocatalytic Degradation

As shown in **Figure 2**, the N doping reaches a maximum at 10 mol% and the

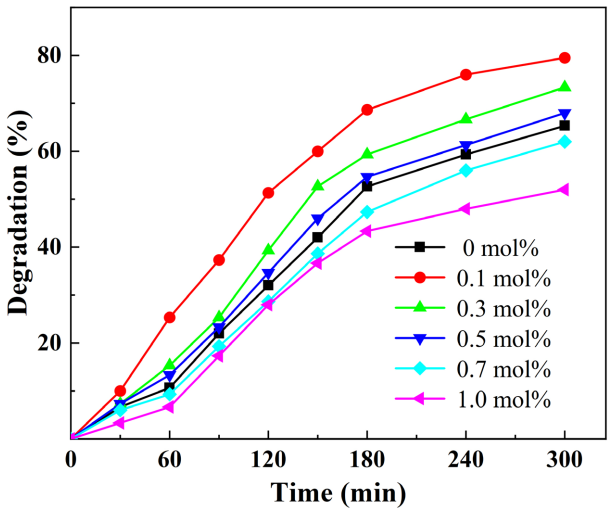

Figure 1. Effect of Ce doping rate on photodegradation of PMG.

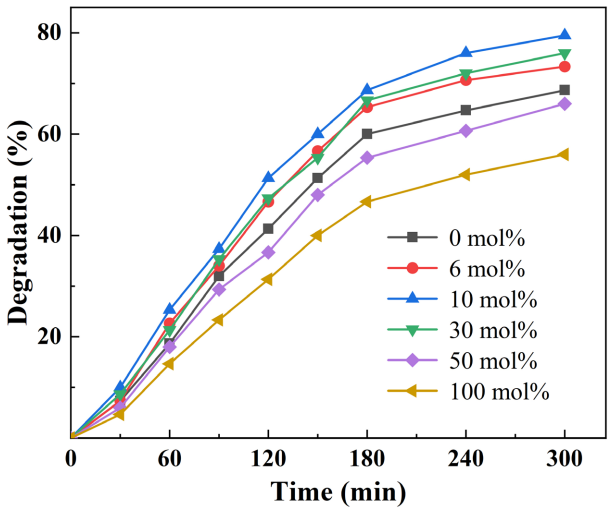

Figure 2. Effect of N doping rate on photodegradation of PMG.

degradation rate of PMG is even inferior to that of the undoped nitrogen photocatalyst after the N doping exceeds 50 mol%. It has been shown [22] [23] [24] that N doping forms a new N 2p energy level band between the TiO_2 conduction and forbidden bands. The valence band electrons can be excited and leap to the impurity energy level N 2p, and then move further to the conduction band, shortening its forbidden band width to make its absorption edge appear red-shifted and improve the photocatalytic efficiency. When the rate of N doping is excessive, it will form deposits on the surface of TiO_2, which will not be uniformly dispersed and the active sites will be covered, thus reducing the photocatalytic activity.

3.1.3. Effect of Calcination Temperature on Photocatalytic Degradation

As can be seen from **Figure 3**, the calcination temperature has a greater effect on the degradation rate of PMG than the Ce and N doping, with the degradation rate of PMG reaching over 80% at 500˚C, however dropping to 40% at 700˚C. When the calcination temperature was low, TiO_2 did not reach the crystallization critical temperature of amorphous phase-anatase, and the photocatalytic degradation performance of the formed amorphous phase TiO_2 was low. When the calcination temperature was too high, firstly, the agglomeration and sintering phenomena on the catalyst surface during the high temperature calcination led to a decrease in the specific surface area of the modified oyster shell powder/Ce-N-TiO_2 composite photocatalyst [25] Secondly, when the calcination temperature is excessive, the rate of nitrogen or cerium doping may be lost and thus affect the effective formation of impurity energy levels [26], reducing the use of visible light portion of the photocatalyst.

3.2. Response Surface Modelling of Modified Oyster Shell Powder/Ce-N-TiO_2

3.2.1. Model Building and Analysis

Based on the Box-Behnken Design (BBD) design response surface test set shown

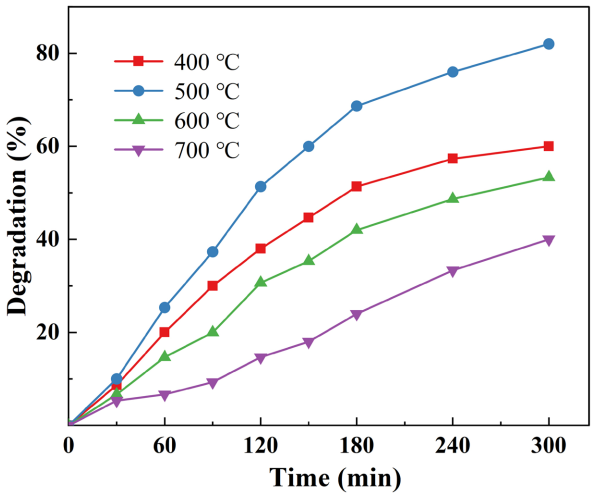

Figure 3. Effect of calcination temperature on photodegradation of PMG.

in Table 2, a ternary linear regression equation with N doping (X_1), Ce doping (X_2) and calcination temperature (X_3) as the response variables and PMG degradation rate (Y) as the response value was established and is shown in Equation (4).

$$Y = 78.80 - 2.52X_1 - 0.9375X_2 + 3.58X_3 + 1.37X_1X_2 + 0.3333X_1X_3 + 0.8333X_2X_3 - 2.30X_1^2 - 2.46X_2^2 - 14.17X_3^2 \quad (4)$$

The results of the preliminary model statistical significance analysis based on analysis of variance (ANOVA) of the model data based on Design-Expert 11.0 software are shown in Table 3. the ANOVA results show a p-value of <0.0001 and an F-value of 101.69, indicating that the model is highly significant; on the other hand, the lack of fit term has an F-value of 2.39 and the response has a p-value of 0.2092 > 0.05, which indicates that the model is not significant in terms of its shortcomings in predicting the data. The X_1, X_2 and X_3 terms in the model were all significant levels, with the interaction term X_1X_2 being more significant, indicating that the three factors selected through the one-way test had a more significant effect on the photocatalytic performance of modified oyster shell powder/Ce-N-TiO_2.

Table 2. Matrix design results in the experiments performed according to the BBD method for PMG removal.

Run	Code			Removal efficiency (%)	
	X_1 (mol%)	X_2 (mol%)	X_3 (˚C)	Actual	Predicted
1	30	0.1	550	65.33	65.85
2	30	0.2	500	78.00	78.80
3	50	0.2	550	63.33	63.73
4	10	0.2	550	68.00	68.10
5	30	0.3	550	66.67	65.64
6	50	0.3	500	71.33	71.96
7	30	0.1	450	59.33	60.35
8	30	0.2	500	80.00	78.80
9	10	0.3	500	73.33	74.25
10	30	0.2	500	78.67	78.80
11	30	0.2	500	79.33	78.80
12	30	0.2	500	78.00	78.80
13	10	0.2	450	62.00	61.60
14	50	0.1	500	72.00	71.08
15	30	0.3	450	57.33	56.81
16	50	0.2	450	56.00	55.90
17	10	0.1	500	79.50	78.88

Table 3. Analysis of variance (ANOVA) for response surface quadratic model applied for modeling PMG removal.

Source	Sum of Squares	df	Mean Square	*F* value	*p* value
Model	1104.27	9	122.70	101.69	<0.0001 (Significant)
X_1-Ce doping	50.84	1	50.84	42.13	0.0003
X_2-Ce doping	7.03	1	7.03	5.83	0.0465
X_3-calcination temperature	102.72	1	102.72	85.14	<0.0001
X_1X_2	7.56	1	7.56	6.27	0.0408
X_1X_3	0.4444	1	0.4444	0..684	0.5631
X_2X_3	2.78	1	2.78	2.30	0.1730
X_1^2	22.19	1	22.19	18.39	0.0036
X_2^2	25.53	1	25.53	21.16	0.0025
X_3^2	845.53	1	845.53	700.78	<0.0001
Residual	8.45	7	1.88		
Lack of Fit	5.42	3	1.81	2.39	0.2092 (Not significant)
Pure Error	3.02	4	0.7556		
Cor Total	1112.72	16			

Based on Pareto analysis, the effect of each independent variable, the interaction effect variable, on the photocatalytic degradation of PMG was assessed [27]. The relative magnitude of the effect of each factor on the response was calculated according to Equation (5) [28] as follows.

$$P_i = \frac{\beta_i^2}{\Sigma\beta_i^2} \tag{5}$$

where β_i denotes the regression coefficient for the linear, quadratic and interaction effects of the response of the second order polynomial. As shown in the Pareto graphical analysis in **Figure 4**, where calcination temperature had the greatest effect on the response, followed by N doping, the interaction effect of X_1X_2 was more pronounced than X_2X_3 and X_1X_3. In summary, the results of the Pareto analysis remained consistent with the results of the ANOVA analysis. The sign of the single factor coefficients in Equation (4) indicates positive or negative effects, and within the range of this study, catalyst calcination temperature has a positive effect, while N and Ce doping are both negative effects; for the crossed product coefficients, positive and negative values represent synergistic and antagonistic effects, respectively, and there are mutual synergistic effects between the three factors within the range of this study.

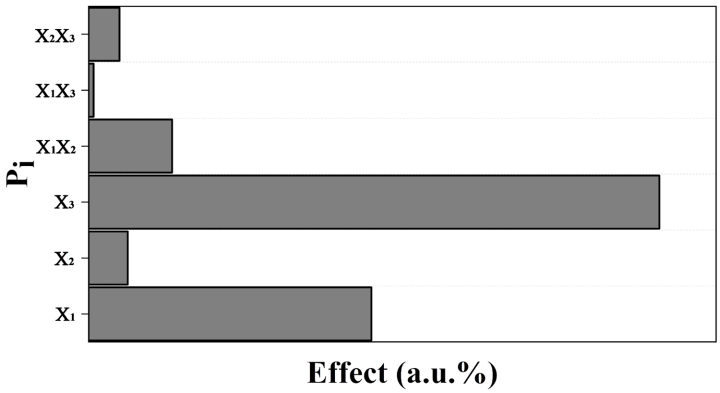

Figure 4. Pareto graph analysis showing the relative effects of the first order, interaction terms of Eq.5 on the photocatalytic reduction of PMG.

3.2.2. Model Validation

In response surface experimental analysis, the model validity depends on a number of assumptions expressed by diagnostic statistics [29] [30], such as scatter plots of actual versus predicted values, scatter plots of studentized residuals versus predicted values, fold plots of studentized residuals versus number of runs and normal probability plots. From **Figure 5(a)**, it is found that the scatter points corresponding to the actual and predicted values are evenly scattered around a certain straight line, indicating that the predicted response is in good agreement with the actual values and that the model shows a good fitting trend. **Figure 5(b)** compares the studentized residual values with the predicted response values and then tests the assumption of constant variance. The scatter plot has some random dispersion, with residuals randomly distributed between the range of [−3, 3]. In addition, the uniform random distribution of each point does not indicate that the variance has a peculiar tendency of linear increase or decrease, so the assumption of constant variance is tenable. **Figure 5(c)** shows the studentized residuals from a model run test, usually used to test hypothetical outliers. The studentized residuals should obey N (0, 1) interval distribution and be approximately independent of each other, and by the nature of the standard normal distribution there exists approximately 95% falling in the range of [−2, 2] horizontal band and further approximately 97% falling in the range [−3, 3] horizontal band [31], whereas **Figure 5(c)** shows that the model studentized residual values fit perfectly and do not show any trend. **Figure 5(d)** is the normal graph of simulation residuals, indicating that the model residuals follow the normal distribution. Obviously, it is proved that it is sufficient to describe the relationship between the research variables and the response values.

From the statistical analysis of the errors, the correlation coefficient R^2 of 0.9924 indicates that the model can explain more than 99.24% of the deviation of the data; the corrected coefficient of determination R^2_{adj} of 0.9827 indicates that there is a high correlation between the experimental and predicted values; the signal-to-noise ratio (Adeq Precision) of 27.2764 is much greater than 4, indicating that the model has sufficient signal and likewise The CV of 1.57% < 10%

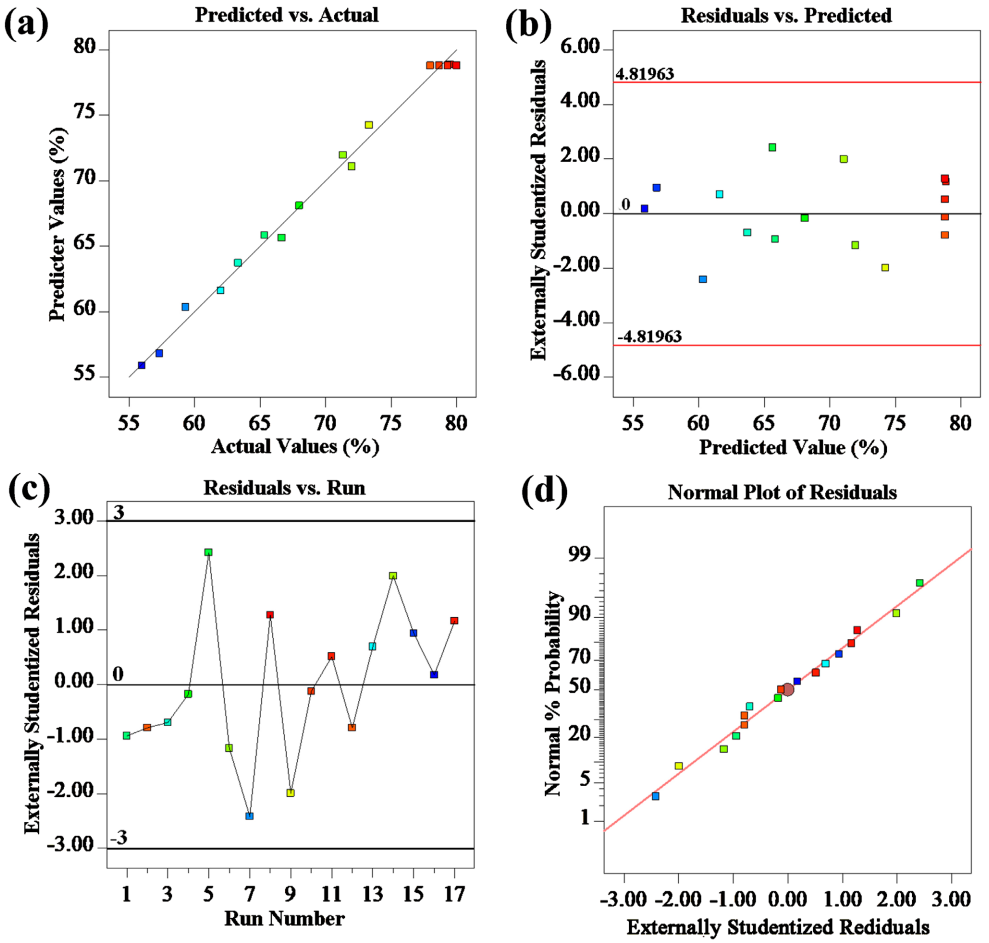

Figure 5. Statistical plots for PMG removal by catalyst: (a) Graph of actual values against predicted ones; (b) The Internally Studentized Residuals against predicted values; (c) The Externally Studentized Residuals against run number; and (d) Normal plot of residuals.

indicates that the test data is accurate and the experimental operation is reliable. In summary, the response surface regression model designed by this central combination can be used to predict the optimal preparation process parameters of modified oyster shell powder/Ce-N-TiO_2 for the degradation of PMG aqueous solution.

3.2.3. Optimized Model Response Surface and Contour Analysis

By fixing one preparation factor parameter, the relationship between the other two preparation parameters and the response can be analyzed by 3D response surface plots and contour plots [32]. **Figure 6** shows the contour and 3D response surface of the degradation rate of PMG solution (150 mL, 50 mg/L, reaction time of 300 min) by simulated Ce doping rate, N doping rate and calcination temperature under fluorescent light.

The contours formed by Ce doping and N doping at a calcination temperature of 500˚C are elliptical, indicating a more significant interaction between the two factors. From the (**Figure 6(a)**, **Figure 6(b)**), the resulting 3D surface has less curvature and is a gentler convex surface, indicating that both have less influence

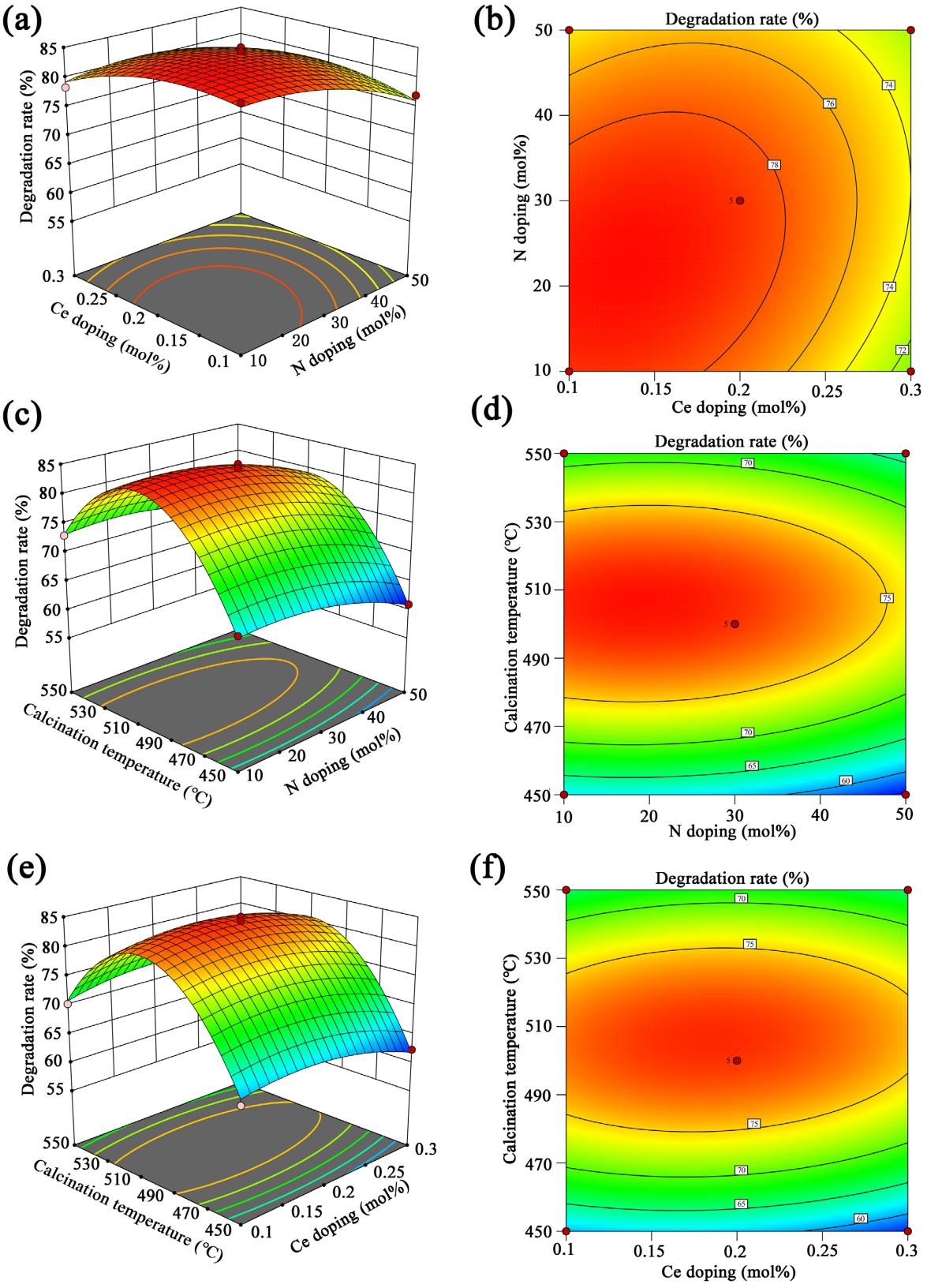

Figure 6. Three-dimensional response surface plots using RSM for PMG photocatalytic reduction: ((a), (b)) Ce doping rate vs. N doping rate; ((c), (d)) N doping rate vs. Calcination temperature; and ((e), (f)) Ce doping rate vs. Calcination temperature.

on the degradation rate within the range of values taken for this test. However, the slope of the N doping curve is steeper and denser compared to the Ce doping curve, indicating a greater contribution of N doping to the effect on response values. This is consistent with the results of comparing the F-values of Ce doping and N doping in Table 3, where the contribution of N doping to the response value is much greater than that of Ce doping.

From the Figures 6(c)-(f), the interaction between N doping and calcination temperature is not significant; the contour plot of Ce doping and calcination temperature is approximately elliptical, indicating that there is some interaction between the two, and this result is more consistent with the results of the p-test in Table 3. The 3D response surface shows that the calcination temperature plays an important role in the degradation of PMG by the photocatalyst, with the degradation rate of PMG solution increasing and then decreasing with the increase in calcination temperature while the Ce or N doping is kept constant, with the maximum response value around 500˚C.

The results of the contour and 3D response surface analysis are consistent with the ANOVA as derived from the graph. Both the steepness of the 3D surface and the F-value showed that the degradation rate of PMG degradation by modified oyster shell powder/Ce-N-TiO_2 was affected in the order of calcination temperature > N-doping rate > Ce-doping rate. The model was solved using Design-Expert 11, and the optimum conditions for the preparation of modified oyster shell powder/Ce-N-TiO_2 to achieve the highest activity in degrading PMG solution were as follows: N doping rate of 17.057 mol%, Ce doping rate of 0.165 mol% and calcination temperature of 505.440˚C. The predicted degradation rate of PMG solution (100 mL, 50 mg/L, 300 min reaction time) was 82.15%. Considering the actual conditions, the optimal preparation conditions were finally determined: N doping rate of 17 mol%, Ce doping rate of 0.165 mol% and calcination temperature of 505˚C.

3.3. Model Validation and Reusability of Catalyst

As shown in Figure 7(a), the photocatalysts were prepared under the optimum conditions, and three replicate tests (150 mL, 50 mg/L, 300 min reaction time) were carried out to degrade PMG under simulated daylight xenon lamp, and the mean value of PMG degradation was 81.51% and the predicted value was 82.15%, with an error rate of 0.64%, which indicated that there was good agreement between the predicted and experimental real values, confirming that the response surface model is reliable

Furthermore, compared to the composite photocatalyst, photocatalytic experiments using the P25 catalyst and Ce-N-TiO_2 under the same conditions were 48.67% and 22% less effective, respectively, indicating that Ce and N doping enabled photocatalytic reactions under visible light and that the addition of modified oyster shell powder resulted in a significant increase in its ability to adsorb pollutants.

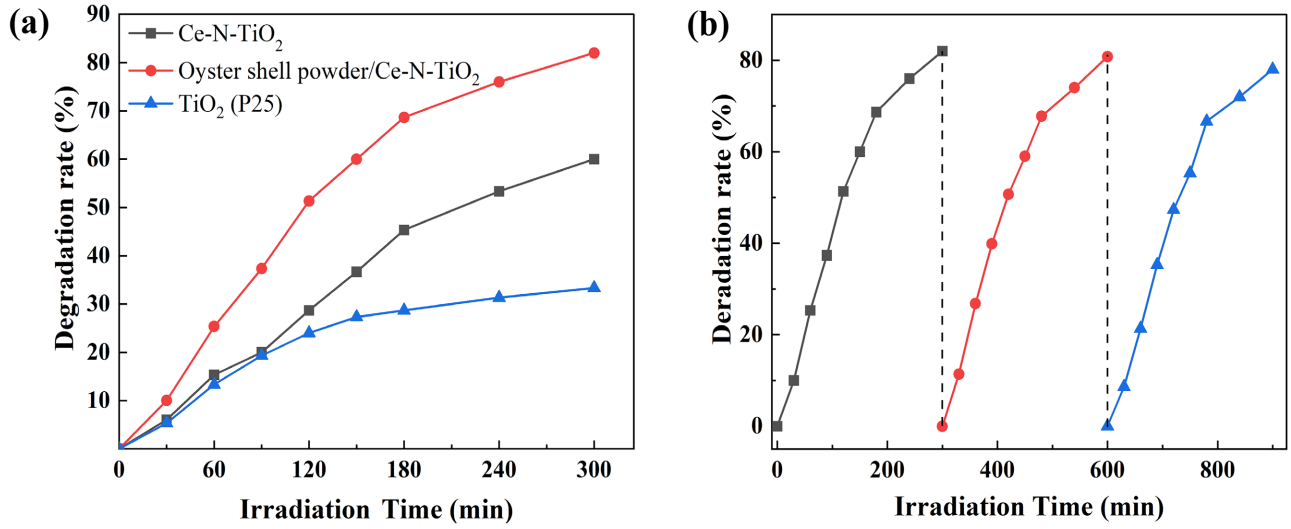

Figure 7. (a) Comparison of PMG degradation rate with TiO_2 (P25) and Ce-N-TiO_2 under optimized conditions; (b) the reproducibility of modified oyster shell powder/Ce-N-TiO_2 catalyst after three times of photocatalytic reduction of PMG.

As the stability of the photocatalyst was equally important, the recycling of modified oyster shell powder/Ce-N-TiO_2 for PMG removal was tested and the results are shown in Figure 7(b). After three cycles, the degradation rate of PMG decreased but was still maintained at around 80%, and the catalyst did not show a significant deactivation trend, indicating that the catalyst has good stability under the experimental conditions studied.

4. Conclusion

Based on the single factor test results, the degradation of PMG by the modified oyster shell powder/Ce-N-TiO_2 under the analog daylight xenon lamp was studied in detail; Box behenken design and response surface methodology (RSM) are used to further optimize and determine the optimal level of the three factors. Compared with the N doping rate, the Ce doping rate and calcination temperature have a greater impact on the photocatalytic process. The interaction between the three is a synergistic effect, and the synergistic interaction between the Ce doping rate and the N doping rate is more obvious. Compared with TiO_2, the photodegradation rate of PMG by the modified oyster shell powder/Ce-N-TiO_2 was improved, which was mainly due to the improvement of adsorption performance and the generation of impurity energy levels to expand the light response range. After three consecutive catalyst cycles, the catalytic activity of the composite photocatalyst didn't decrease significantly. The results showed that the response surface model was an effective tool to optimize the preparation conditions of the modified oyster shell powder/Ce-N-TiO_2.

Acknowledgments

We are grateful to National Natural Science Foundation of China (No.42071122) for financial support.

Conflicts of Interest

The authors declare no conflicts of interest regarding the publication of this paper.

References

[1] Espinoza-Montero, P.J., Vega-Verduga, C., Alulema-Pullupaxi, P., Fernández, L. and Paz, J.L. (2020) Technologies Employed in the Treatment of Water Contaminated with Glyphosate: A Review. *Molecules*, **25**, Article No. 5550. https://doi.org/10.3390/molecules25235550

[2] Tresnakova, N., Stara, A. and Velisek, J. (2021) Effects of Glyphosate and Its Metabolite AMPA on Aquatic Organisms. *Applied Sciences*, **11**, Article No. 9004. https://doi.org/10.3390/app11199004

[3] Kanissery, R., Gairhe, B., Kadyampakeni, D., Batuman, O. and Alferez, F. (2019) Glyphosate: Its Environmental Persistence and Impact on Crop Health and Nutrition. *Plants*, **8**, Article No. 499. https://doi.org/10.3390/plants8110499

[4] Van Bruggen, A.H.C., He, M.M., Shin, K., *et al.* (2018) Environmental and Health Effects of the Herbicide Glyphosate. *Science of the Total Environment*, **616-617**, 255-268. https://doi.org/10.1016/j.scitotenv.2017.10.309

[5] Bonansea, R.I., Filippi, I., Wunderlin, D.A., Marino, D.J.G. and Amé, M.V. (2017) The Fate of Glyphosate and AMPA in a Freshwater Endorheic Basin: An Ecotoxicological Risk Assessment. *Toxics*, **6**, Article No. 3. https://doi.org/10.3390/toxics6010003

[6] Gopinath, K.P., Madhav, N.V., Krishnan, A., Malolan, R. and Rangarajan, G. (2020) Present Applications of Titanium Dioxide for the Photocatalytic Removal of Pollutants from Water: A Review. *Journal of Environmental Management*, **270**, Article ID: 110906. https://doi.org/10.1016/j.jenvman.2020.110906

[7] Kanakaraju, D., Glass, B.D. and Oelgemoller, M. (2018) Advanced Oxidation Process-Mediated Removal of Pharmaceuticals from Water: A Review. *Journal of Environmental Management*, **219**, 189-207. https://doi.org/10.1016/j.jenvman.2018.04.103

[8] Giannakis, S., Rtimi, S. and Pulgarin, C. (2017) Light-Assisted Advanced Oxidation Processes for the Elimination of Chemical and Microbiological Pollution of Wastewaters in Developed and Developing Countries. *Molecules*, **22**, Article No. 1070. https://doi.org/10.3390/molecules22071070

[9] Du, Y.-B., Zhang, L., Ruan, M., Niu, C.-G., *et al.* (2018) Template-Free Synthesis of Three-Dimensional Porous CdS/TiO_2 with High Stability and Excellent Visible Photocatalytic Activity. *Materials Chemistry and Physics*, **212**, 69-77. https://doi.org/10.1016/j.matchemphys.2018.03.033

[10] Poo-Arporn, Y., Kityakarn, S., Niltharach, A., *et al.* (2019) Photocatalytic Oxidation of Thiophene over Cerium Doped TiO_2 Thin Film. *Materials Science in Semiconductor Processing*, **93**, 21-27. https://doi.org/10.1016/j.mssp.2018.12.025

[11] Le, T.T.T., Tran, D.T. and Danh, T.H. (2021) Remarkable Enhancement of Visible Light Driven Photocatalytic Performance of TiO_2 by Simultaneously Doping with C, N, and S. *Chemical Physics*, **545**, Article ID: 111144. https://doi.org/10.1016/j.chemphys.2021.111144

[12] Aba-Guevara, C.G., Medina-Ramírez, I.E., Hernández-Ramírez, A., *et al.* (2017) Comparison of Two Synthesis Methods on the Preparation of Fe,N-Co-Doped TiO_2 Materials for Degradation of Pharmaceutical Compounds under Visible Light. *Ceramics International*, **43**, 5068-5079. https://doi.org/10.1016/j.ceramint.2017.01.018

[13] He, S., Yang, Z., Cui, X., Zhang, X. and Niu, X. (2020) Fabrication of the Novel Ag-Doped SnS_2@$InVO_4$ Composite with High Adsorption-Photocatalysis for the Removal of Uranium (VI). *Chemosphere*, **260**, Article ID: 127548. https://doi.org/10.1016/j.chemosphere.2020.127548

[14] Dagde, K.K. (2018) Biosorption of Crude Oil Spill Using Groundnut Husks and Plantain Peels as Adsorbents. *Advances in Chemical Engineering and Science*, **8**, 161-175. https://doi.org/10.4236/aces.2018.83011

[15] Jiang, N., Shang, R., Heijman, S.G.J. and Rietveld, L.C. (2018) High-Silica Zeolites for Adsorption of Organic Micro-Pollutants in Water Treatment: A Review. *Water Research*, **144**, 145-161. https://doi.org/10.1016/j.watres.2018.07.017

[16] Wang, N., Hao, L., Chen, J., Zhao, Q. and Xu, H. (2018) Adsorptive Removal of Organics from Aqueous Phase by Acid-Activated Coal Fly Ash: Preparation, Adsorption, and Fenton Regenerative Valorization of "Spent" Adsorbent. *Environmental Science and Pollution Research*, **25**, 12481-12490. https://doi.org/10.1007/s11356-018-1560-y

[17] Alvarez-García, S., Ramírez-García, J.J., Granados-Correa, F. and Sánchez-Meza, J.C. (2019) Structural and Textural Influences of Surfactant-Modified Zeolitic Materials over the Methamidophos Adsorption Behavior. *Separation Science and Technology*, **55**, 619-634. https://doi.org/10.1080/01496395.2019.1568476

[18] Wang, J., Wang, X., Qiu, L., Li, T. and Yu, C. (2018) Study on Key Factors of Adsorption of Phosphorus by Steel Slag Filter Based on Response Surface Method. *E3S Web of Conferences*, **53**, Article No. 03050. https://doi.org/10.1051/e3sconf/20185303050

[19] Cao, Y., Fan, Y., Ma, Z., *et al.* (2018) Urea-Functionalized SBA-15 Hybrids: Post-Grafting Synthesis, High-Performance Organophosphorus Sensing and Their Response Mechanism. *Sensors and Actuators B*: *Chemical*, **273**, 1162-1169. https://doi.org/10.1016/j.snb.2018.04.112

[20] Chaker, H., Fourmentin, S. and Chérif-Aouali, L. (2020) Efficient Photocatalytic Degradation of Ibuprofen under Visible Light Irradiation Using Silver and Cerium Co-Doped Mesoporous TiO_2. *ChemistrySelect*, **5**, 11787-11796. https://doi.org/10.1002/slct.202002730

[21] Belver, C., Bedia, J., Álvarez-Montero, M.A. and Rodriguez, J.J. (2016) Solar Photocatalytic Purification of Water with Ce-Doped TiO_2/Clay Heterostructures. *Catalysis Today*, **266**, 36-45. https://doi.org/10.1016/j.cattod.2015.09.025

[22] Than, L.D., Luong, N.S., Ngo, V.D., *et al.* (2016) Highly Visible Light Activity of Nitrogen Doped TiO_2 Prepared by Sol–Gel Approach. *Journal of Electronic Materials*, **46**, 158-166. https://doi.org/10.1007/s11664-016-4894-6

[23] Mohamed, M.A., Salleh, W.N.W., Jaafar, J., *et al.* (2016) Physicochemical Characteristic of Regenerated Cellulose/N-Doped TiO_2 Nanocomposite Membrane Fabricated from Recycled Newspaper with Photocatalytic Activity under UV and Visible Light Irradiation. *Chemical Engineering Journal*, **284**, 202-215. https://doi.org/10.1016/j.cej.2015.08.128

[24] Bakar, S.A., Byzynski, G. and Ribeiro, C. (2016) Synergistic Effect on the Photocatalytic Activity of N-Doped TiO_2 Nanorods Synthesised by Novel Route with Exposed (110) Facet. *Journal of Alloys and Compounds*, **666**, 38-49. https://doi.org/10.1016/j.jallcom.2016.01.112

[25] Suwannaruang, T., Kamonsuangkasem, K., Kidkhunthod, P., *et al.* (2018) Influence of Nitrogen Content Levels on Structural Properties and Photocatalytic Activities of Nanorice-Like N-Doped TiO_2 with Various Calcination Temperatures. *Materials*

Research Bulletin, **105**, 265-276. https://doi.org/10.1016/j.materresbull.2018.05.010

[26] Wang, C., Ao, Y., Wang, P., Hou, J. and Qian, J. (2011) Preparation of Cerium and Nitrogen Co-Doped Titania Hollow Spheres with Enhanced Visible Light Photocatalytic Performance. *Powder Technology*, **210**, 203-207. https://doi.org/10.1016/j.powtec.2011.03.015

[27] Antonopoulou, M., Chondrodimou, I., Bairamis, F., Giannaka, A. and Konstantinou, I. (2017) Photocatalytic Reduction of Cr(VI) by Char/TiO_2 Composite Photocatalyst: Optimization and Modeling Using the Response Surface Methodology (RSM). *Environmental Science and Pollution Research*, **24**, 1063-1072. https://doi.org/10.1007/s11356-016-6779-x

[28] Fathinia, M., Khataee, A.R., Zarei, M. and Aber, S. (2010) Comparative Photocatalytic Degradation of Two Dyes on Immobilized TiO_2 Nanoparticles: Effect of Dye Molecular Structure and Response Surface Approach. *Journal of Molecular Catalysis A*: *Chemical*, **333**, 73-84. https://doi.org/10.1016/j.molcata.2010.09.018

[29] Mousavi, M., Soleimani, M., Hamzehloo, M., Badiei, A. and Ghasemi, J.B. (2021) Photocatalytic Degradation of Different Pollutants by the Novel gCN-NS/Black-TiO_2 Heterojunction Photocatalyst under Visible Light: Introducing a Photodegradation Model and Optimization by Response Surface Methodology (RSM). *Materials Chemistry and Physics*, **258**, Article ID: 123912. https://doi.org/10.1016/j.matchemphys.2020.123912

[30] Rahimi, B. and Ebrahimi, A. (2019) Photocatalytic Process for Total Arsenic Removal Using an Innovative BiVO4/TiO_2/LED System from Aqueous Solution: Optimization by Response Surface Methodology (RSM). *Journal of the Taiwan Institute of Chemical Engineers*, **101**, 64-79. https://doi.org/10.1016/j.jtice.2019.04.036

[31] Rahimi, B., Jafari, N., Abdolahnejad, A., Farrokhzadeh, H. and Ebrahimi, A. (2019) Application of Efficient Photocatalytic Process Using a Novel BiVO/TiO_2-NaY Zeolite Composite for Removal of Acid Orange 10 Dye in Aqueous Solutions: Modeling by Response Surface Methodology (RSM). *Journal of Environmental Chemical Engineering*, **7**, Article ID: 103253. https://doi.org/10.1016/j.jece.2019.103253

[32] Das, B., Banerjee, S., Raul, P.K., *et al.* (2021) Removal of Fluoride from Water Using Mesoporous MCM-41: An Optimization Approach Using Response Surface Methodology (RSM). *Advances in Nanoparticles*, **10**, 95-114. https://doi.org/10.4236/anp.2021.103007